Nanomaterials

DOI: 10.1002/anie.201209736

Carbon Nanotubes Bridged with Graphene Nanoribbons and Their Use in High-Efficiency Dye-Sensitized Solar Cells**

Zhibin Yang, Mingkai Liu, Chao Zhang, Weng Weei Tjiu, Tianxi Liu, and Huisheng Peng**

To improve the practical application of functional nanomaterials, it is critically important, but often challenging, to extend their excellent properties from the nanoscale to the macroscopic scale.[1] For example, carbon nanotubes (CNTs) have been widely studied as a new family of electrode materials for various optoelectronic and electronic devices, owing to their unique structure and remarkable electronic and catalytic properties.[2–11] However, CNTs were typically aggregated to form networks with many boundaries, which significantly inhibited rapid charge transport. The resulting CNT-based electrodedevices showed much lower efficiency than expected.[5]

To solve the above problem and achieve high performance at the macroscopic scale, a general strategy is to design novel structures to realize effective interactions among CNTs at the molecular scale. To this end, nature provides excellent models for efficiently performing complex functions through the creation of elaborate structures. Well-known examples are blood vessels, which are constructed with trunks interconnected by a lot of branches, a paradigmatic structure to rapidly deliver nutrients throughout our bodies. Inspired by nature, herein we discuss the development of a new structure in which CNTs are bridged by graphene nanoribbons. Briefly, multiwalled CNTs are partially unzipped to form nanoribbons with one end on the mother CNT and the other on a neighboring CNT. Due to the strong π–π interaction between nanotube and nanoribbon, and the high charge mobility in nanoribbons,[12–15] produced electrons can be rapidly transported among CNTs to macroscopically achieve high performance. As a demonstration, dye-sensitized solar cells (DSCs) with graphene-nanoribbon-bridged CNTs as counter electrodes (Figure 1) showed an energy conversion efficiency of up to 8.23 %, compared with 7.61 % for a conventional platinum counter electrode under similar conditions.

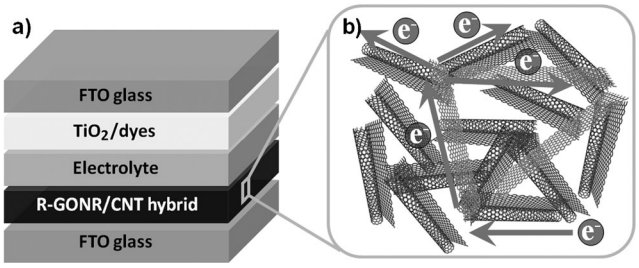

Figure 1. a) the structure of dye-sensitized solar cells based on R-GONR-bridged CNTs as counter electrode. b) the mechanism of rapid electron transport in the counter electrode.

Multiwalled CNTs with a diameter of 20–40 nm and a wall number of 20–30 were primarily studied (Supporting Information, SFigure S1). The CNTs were chemically unzipped to produce graphene oxide nanoribbons (GONRs; Figure S2). The degree of unzipping could mainly be increased by increasing the amount of potassium permanganate. X-ray diffraction (XRD) analysis was undertaken to quantitatively determine the degree of unzipping. Figure S3 shows typical XRD patterns for the mixtures of GONR and CNT with different GONR weight percentages. As the amount of GONR in the mixture increased, the characteristic GONR peak ($2\theta = 11.2°$) gradually increased while the CNT peak ($2\theta = 26.1°$) gradually decreased.[13] Based on the intensity of their characteristic peaks, a relationship curve between GONR weight percentage and intensity ratio was obtained. This curve could be then used to calculate the weight percentage of GONRs in the resulting hybrid (Figure S4). Figure 2 compares the XRD patterns of pristine CNTs, GONR/CNT hybrids with different GONR weight percentages, and pure GONR. The GONR weight percentages in three hybrid samples were calculated as approximately 16 %, 55 %, and 85 %. For simplicity, they were defined as $GONR_{16\%}$/CNT, $GONR_{55\%}$/CNT and $GONR_{85\%}$/CNT. CNTs could be also completely unzipped to form pure nanoribbons.

Raman spectroscopy was used to monitor structural changes during the unzipping process of CNTs (Figure S5). The D band at ca. 1350 cm^{-1} gradually broadened and increased in intensity as the reaction progressed, a result which corresponds to increasing GONR weight percentage. As a result, the ratio between the intensities of the D and G bands (I_D/I_G) was enhanced, which indicates a decrease in

[*] Z. Yang,[+] M. Liu,[+] C. Zhang, Prof. T. Liu, Prof. H. Peng
State Key Laboratory of Molecular Engineering of Polymers and Department of Macromolecular Science, Fudan University
Shanghai 200433 (China)
E-mail: txliu@fudan.edu.cn
penghs@fudan.edu.cn
Z. Yang,[+] Prof. H. Peng
Laboratory of Advanced Materials, Fudan University
Shanghai 200438 (China)
W. W. Tjiu
Institute of Materials Research and Engineering, A*STAR (Agency for Science, Technology and Research)
3 Research Link, Singapore, 117602 (Singapore)
[+] These authors contributed equally to this work.

[**] This work was financially supported by the National Natural Science Foundation of China (51125011, 91027025, 21225417), MOST (2011CB932503, 2011DFA51330), STCSM (11520701400, 12nm0503200), and the Program for Prof. of Special Appointment at the Shanghai Institutions of Higher Learning.
Supporting information for this article is available on the WWW under http://dx.doi.org/10.1002/anie.201209736.

© 2013 Wiley-VCH Verlag GmbH & Co. KGaA, Weinheim

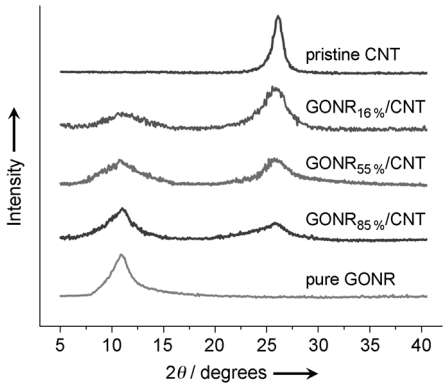

Figure 2. XRD patterns of pristine CNTs, GONR/CNT hybrids with different GONR weight percentages, and pure GONRs.

the average sp^2 domain sizes.[16] Fourier-transform infrared spectroscopy (FTIR) and thermogravimetric analysis (TGA) were also used to verify the Raman results. The vibration intensities of oxygen-containing groups (such as C=O at ca. 1730 cm^{-1}) were gradually increased during the reaction (Figure S6). At the same time, the weight loss of the resulting material was increased as the amount of GONR increased (Figure S7).

The GONR/CNT hybrids and pure GONR had been deoxygenated by hydroiodic acid, which was verified by FTIR and TGA analysis. For example, compared with the $GONR_{16\%}$/CNT hybrid, no obvious vibrations for oxygen-containing groups were found after reduction (Figure S8). For the convenience of discussion, the reduced sample was called R-$GONR_{16\%}$/CNT. The R-$GONR_{16\%}$/CNT hybrid showed a higher thermal stability (a weight loss of 7% vs. 11% for the $GONR_{16\%}$/CNT; Figure S9), which further showed a successful reduction of $GONR_{16\%}$/CNT.[17]

The GONR/CNT hybrid materials were further analyzed by X-ray photoelectron spectroscopy (XPS). No potassium had been detected in the XPS spectra (Figure S10a). The structure evolution of the hybrid material after reduction was further verified by tracing the relative peak intensities of C–C/C=C (284.9 eV) and C–O (286.5 eV)/C=O (288.3 eV) groups (Figure S10b and S11e); the C–O/C=O peaks were significantly decreased after reduction. The structures of R-GONR/CNT hybrid materials were also compared with both pristine CNTs and R-GONRs by XPS (Figure S11). The oxygen content increased as the degree of unzipping increased, as more oxygen-containing groups were introduced during the unzipping process.

The R-$GONR_{16\%}$/CNT hybrid was studied by transmission electron microscopy (TEM) and scanning electron microscopy (SEM). Figure 3 compares pristine CNTs, R-GONR/CNT hybrids with different R-GONR weight percentages, and pure R-GONR. More and more R-GONRs were observed in the hybrid as the degree of unzipping increased. As expected, the unzipped nanoribbons were attached to various CNTs in the R-GONR/CNT hybrid, which resulted in excellent electronic properties, for example, electrical conductivities on the level of 10^2 S cm^{-1}. Here the conductivity of the R-$GONR_{16\%}$/CNT hybrid film was two

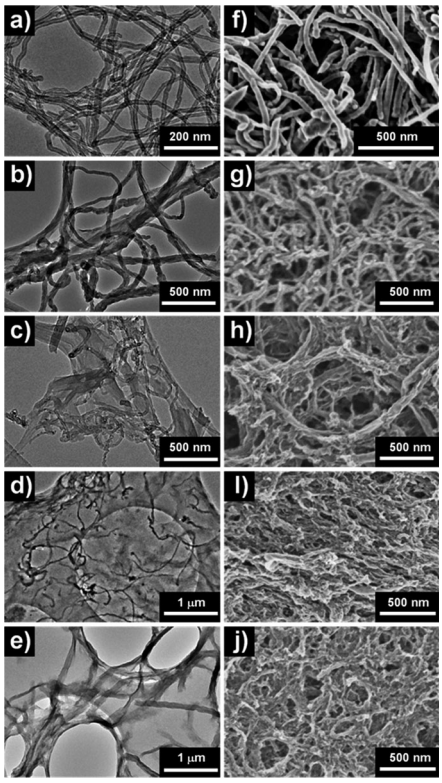

Figure 3. a–e) TEM images of pristine CNTs, R-GONR/CNT hybrids with increasing R-GONR weight percentages (16%, 55%, 85%), and pure R-GONR, respectively. f–j), SEM images corresponding to (a–e), respectively.

times that of the pure CNT film and three times that of the pure R-GONR film. Moreover, the conductivities of the R-GONR/CNT hybrid films gradually decreased as the R-GONR weight percentage increased.

R-GONR/CNT hybrid materials may represent a new family of electrode materials. Herein, they were mainly explored as replacements for conventional platinum counter electrodes in DSCs. To this end, pristine CNTs, R-GONR/CNT hybrids with different R-GONR weight percentages, and pure R-GONR electrodes prepared by a spin-coating method were first compared for catalytic activities. They were studied by cyclic voltammetry (CV) measurements in an acetonitrile solution containing I_2, LiI, and $LiClO_4$.[6,18] As shown in Figure 4a, two pairs of oxidation/reduction peaks, A_{OX}/A_{RE} and B_{OX}/B_{RE}, were observed in the CV curves for each counter electrode. The A_{OX}/A_{RE} and B_{OX}/B_{RE} redox pairs correspond to the reactions in Equation (1) and (2), respectively.

$$I_3^- + 2e^- \rightleftharpoons 3I^- \quad (1)$$

$$3I_2 + 2e^- \rightleftharpoons 3I_3^- \quad (2)$$

Generally, the catalytic activity of an electrode is related to the A_{OX}/A_{RE} redox pair. A higher reduction peak current density (J_{RE}) and a lower peak-to-peak voltage separation (V_{PP}) indicate a higher catalytic activity.[19] As electrode materials with high specific areas (such as CNTs) always show

 © 2013 Wiley-VCH Verlag GmbH & Co. KGaA, Weinheim

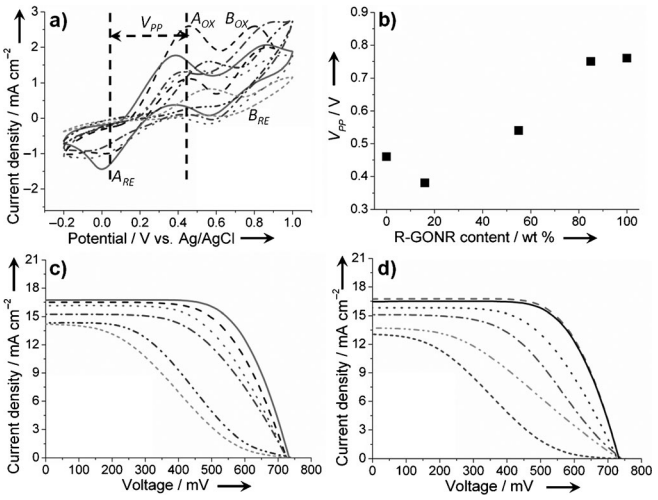

Figure 4. a) Electrocatalytic characterization of pristine CNTs (–•–•), R-GONR/CNT hybrids with different RNR weight percentages (16%, ——; 55%, •••••; 85%, –••••), pure R-GONR (-----), and platinum (– – –). b) V_{PP} values corresponding to the materials in (a), except for Pt. c) *J–V* characteristics of the DSC with pristine CNTs (–•–•), R-GONR/CNT hybrids with different RNR weight percentages (16%, ——; 55%, •••••; 85%, –••••), pure R-GONR (-----), and platinum (– – –) as counter electrodes measured under AM 1.5 illumination. d) *J–V* characteristics of DSCs based on R-GONR$_{16\%}$/CNT hybrids with different thicknesses as counter electrodes measured under AM 1.5 illumination. Approximate thicknesses: 1 μm (——), 500 nm (– – –), 300 nm (•••••), 200 nm (–•–•), 100 nm (–••••), 50 nm (-----).

a high J_{RE}, it is more effective to investigate their catalytic activities by comparing their V_{PP} values. The V_{PP} of R-GONR$_{16\%}$/CNT hybrid was 0.38 V, a value which is lower than that pure CNT (0.46 V), and even lower than that of platinum (0.41 V; Figure 4b). Therefore, the R-GONR$_{16\%}$/CNT hybrid electrode may be the most effective in the reduction of I_3^-. Note that the V_{PP} values increased as the R-GONR weight percentage increased.

The above electrodes were used as counter electrodes to fabricate DSCs. Fluorine-doped tin oxide (FTO) glass deposited with TiO_2 nanoparticles was used as the working electrode, and *cis*-diisothiocyanato-bis(2,2′-bipyridyl-4,4′-dicarboxylato) ruthenium(II) bis(tetrabutylammonium) (N719) was used as the dye. Figure 4c shows typical *J–V* curves measured under AM 1.5 illumination, and the photovoltaic parameters are summarized at Table S1. The devices shared almost the same open-circuit voltage (V_{OC}) of ca. 0.73 V, but exhibited different short-circuit current density (J_{SC}) and filling factor (FF) values. For the R-GONR$_{16\%}$/CNT hybrid electrode, the energy conversion efficiency of the resulting DSC was 8.23%, a value which is much higher than that of pristine CNT (6.09%). This result agrees well with the bridged structure, where electrons are rapidly transported along the R-GONR bridges among CNTs from the inner side to the conductive substrate.

To further verify the importance of this partial-unzipping method to produce a bridged structure that favors close and effective contacts between R-GONRs and CNTs, pure R-GONRs and pure CNTs were directly mixed in solution and then coated onto films that were then also used as counter electrodes to fabricate DSCs. The resulting DSC showed a V_{OC} of 0.731 V, a J_{SC} of 14.28 mA cm^{-2}, and an FF of 0.60. The energy conversion efficiency was calculated to be 6.23% (Figure S12), which is much lower than the R-GONR$_{16\%}$/CNT hybrid electrode prepared by the unzipping process. This phenomenon may be explained by the fact that R-GONRs and CNTs tend to aggregate, and so the CNTs were not effectively bridged by the R-GONRs.

As another point of comparison, a DSC fabricated with a conventional platinum counter electrode showed an efficiency of 7.61% (Figure 4c), which was also lower than the R-GONR$_{16\%}$/CNT hybrid. Although it may be not be accurate to directly compare the hybrid with platinum, as the hybrid electrode has a much higher surface area (owing to its nanostructure) than the platinum, this comparison at least indicates that the hybrid materials are promising for use as counter electrodes in DSCs. In particular, these hybrid electrodes could be easily synthesized at low cost and on a large scale.

The DSCs fabricated with counter electrodes of R-GONR/CNT hybrids with different R-GONR weight percentages were also compared. Both J_{SC} and FF values decreased as the R-GONR weight percentage increased, although the V_{OC} values remained similar. Therefore, as the R-GONR weight percentage increased (16, 55, and 85%) the energy conversion efficiencies decreased (8.23, 6.85, and 3.98%, respectively). More CNT walls were completely unzipped to form free R-GONRs, and the free R-GONRs largely decreased the π–π interactions among partially unzipped CNTs as they competed to stack with the partially unzipped CNTs and aggregated with each other. Furthermore, pure
R-GONR showed a much lower efficiency of 3.31%. Therefore, completely unzipped R-GONR would decrease cell efficiencies, although partially unzipped R-GONR increases them. As a result of this observation, an optimal average degree of unzipping, which corresponds to an R-GONR weight percentage of ca. 16%, was determined.

To further improve DSC efficiency, the dependence of DSC performance on hybrid electrode thickness was also studied. Figure 4d compares R-GONR$_{16\%}$/CNT hybrids with different thicknesses (the photovoltaic parameters are summarized in Table S2). As thickness increased from 50 nm to 500 nm, the V_{OC} values remained almost unchanged at ca. 0.73 V, while J_{SC} and FF increased from 12.98 mA cm^{-2} to 16.73 mA cm^{-2} and from 0.27 to 0.67, respectively. Both J_{SC} and FF reached platforms as electrode thickness was increased further. The optimal thickness of the R-GONR$_{16\%}$/CNT hybrid electrode was determined to be ca. 500 nm.

The R-GONR/CNT hybrid films can also be highly transparent and flexible (Figure S13–S17). Figure S13 compares the R-GONR$_{16\%}$/CNT hybrid film and a glass slide over a marked paper. In both cases, the underlying words could be clearly observed. The flexibility was verified by bending the hybrid film to different bending radii and with increasing cycle numbers (Figure S15 and S16). The resistances remained almost unchanged during the above processes. The relationship between resistance and transmittance in the

 © 2013 Wiley-VCH Verlag GmbH & Co. KGaA, Weinheim

hybrid film is also shown in Figure S17. As expected, the sheet resistances decreased as transmittance decreased. Here the film thickness was varied between 50 and 250 nm. As a demonstration of application, the flexible hybrid film was used as a counter electrode to fabricate flexible DSCs with an efficiency of 2.44% (Figure S18). These transparent and flexible hybrid films also show promising applications as electrodes in a wide variety of optoelectronic devices, such as solar cells and organic light-emitting diodes. Note that the chemical composition, density, and alignment played critical roles in the resistance of hybrid films. Currently, the minimum sheet resistance is about 100 Ω. Efforts are underway to further decrease it.

In summary, through an easy solution process, we have created a novel structure consisting of CNTs bridged by R-GONRs. This material favors rapid charge transport among CNTs, resulting in high performance at the macroscopic scale. When used as counter electrodes, the resulting DSCs showed high energy conversion efficiencies of up to 8.23%. This work also provides a paradigmatic structural design for high performance optoelectronic and electronic devices.

Experimental Section

Electrodes from R-GONR/CNT hybrid and pure R-GONR materials: Multiwalled CNTs (0.2 g) were dispersed in concentrated sulfuric acid (50 mL) by stirring for 1.5 h, followed by the addition of phosphoric acid (7 mL) under stirring for 20 min. At the same time, the mixture temperature was gradually increased to 70°C. Different reaction solutions were then produced by the addition of 0.3, 0.5, 0.7, or 0.9 g of powdered potassium permanganate, as desired, with each addition conducted at a rate of about 0.2 g per hour. The final mixtures were allowed to cool to room temperature and slowly dropped into 300 mL of ice water containing H_2O_2 (10 mL; 30 wt%). The resulting solids were redispersed in deionized H_2O and dialyzed for a week until the pH was close to 7. The solutions were further centrifuged at 8000 rpm for 10 min, followed by vigorous sonication for 15 min. The resulting homogenous solutions were filtered by polytetrafluoroethylene membranes with a pore size of 0.22 μm to obtain either a GONR/CNT hybrid with different GONR weight percentages or pure GONR. To synthesize reduced graphene materials, the GONR/CNT hybrid or pure GONR was immersed in an aqueous solution of HI (55%) in a sealed flask for 8 h at 100°C, followed by dialysis with deionized water to remove the residual reduction agents. The resulting R-GONR/CNT or pure GRN materials could be homogenously dispersed in dimethylformamide (2 mg mL^{-1}) and then spin-coated onto FTO. The thicknesses were controlled by the spinning speed and number of cycles. For example, a thickness of ca. 50 nm was obtained at a speed of 1500 rpm with a 1 mg mL^{-1} of hybrid solution.

Fabrication of DSCs: The hybrid counter electrodes were heated at 500°C in argon for 30 min for better contact. In the case of a platinum counter electrode, it was prepared by coating H_2PtCl_6 onto FTO glass, followed by thermal decomposition at 500°C in air for 30 min. The working electrode was composed of a layer of nanocrystalline TiO_2 (diameter of 20 nm) with a thickness of 14 μm and a light-scattering layer of TiO_2 (diameter of 200 nm) with a thickness of 2 μm prepared by screen printing technology. The surface area of the TiO_2 electrodes was 0.36 cm^2. The working electrode was heated to 500°C for 30 min and annealed in air. It was then immersed in an aqueous solution of $TiCl_4$ (40 mM) at 70°C for 30 min and washed with deionized water and ethanol, followed by sintering at 500°C for 30 min. After the temperature was decreased to 120°C, it was immersed into an N719 solution (0.3 mM) in dry acetonitrile and *tert*-butanol (1:1) for 16 h. The N719-incorporated electrode was carefully rinsed with dry acetonitrile. The working and counter electrodes with a Surlyn frame as the spacer were sealed by pressing them together at a pressure of about 0.2 MPa and a temperature of 125°C. The redox electrolyte (composed of 0.1M lithium iodide, 0.05M iodine, 0.6M 1, 2-dimethyl-3-propylimidazolium iodide and 0.5M 4-*tert* butyl-pyridine in dry acetonitrile) was introduced into the cell through the back hole of the counter electrode. Finally, the hole was sealed with the Surlyn and a cover glass. In the case of a flexible DSC, a mixture of 80% anatase and 20% rutile TiO_2 was added to ethanol (20 wt%). The suspension was coated onto the conducting substrate by a doctor-blading method to produce the working electrode.

Received: December 5, 2012
Revised: January 8, 2013
Published online: February 11, 2013

Keywords: carbon · dye-sensitized solar cells · graphene · nanoribbons · nanotubes

[1] a) X. Sun, T. Chen, Z. Yang, H. Peng, *Acc. Chem. Res.* **2013**, DOI: 10.1021/ar300221r; b) H. Peng, *J. Am. Chem. Soc.* **2008**, *130*, 42–43; c) Z. Yang, X. Sun, X. Chen, Z. Yong, G. Xu, R. He, Z. An, Q. Li, H. Peng, *J. Mater. Chem.* **2011**, *21*, 13772–13775; d) T. Chen, S. Wang, Z. Yang, Q. Feng, X. Sun, L. Li, Z. S. Wang, H. Peng, *Angew. Chem.* **2011**, *123*, 1855–1859; *Angew. Chem. Int. Ed.* **2011**, *50*, 1815–1819.
[2] S. Cataldo, P. Salice, E. Menna, B. Pignataro, *Energy Environ. Sci.* **2012**, *5*, 5919–5940.
[3] Y. Feng, X. Ju, W. Feng, H. Zhang, Y. Cheng, J. Liu, A. Fujii, M. Ozaki, K. Yoshino, *Appl. Phys. Lett.* **2009**, *94*, 123302.
[4] C. Berger, Y. Yi, Z. Wang, W. De Heer, *Appl. Phys. A* **2002**, *74*, 363–365.
[5] Z. Yang, T. Chen, R. He, G. Guan, H. Li, L. Qiu, H. Peng, *Adv. Mater.* **2011**, *23*, 5436–5439.
[6] T. Chen, L. Qiu, H. G. Kia, Z. Yang, H. Peng, *Adv. Mater.* **2012**, *24*, 4623–4628.
[7] S. Ng, J. Wang, Z. Guo, J. Chen, G. Wang, H. Liu, *Electrochim. Acta* **2005**, *51*, 23–28.
[8] Z. Fan, J. Yan, L. Zhi, Q. Zhang, T. Wei, J. Feng, M. Zhang, W. Qian, F. Wei, *Adv. Mater.* **2010**, *22*, 3723–3728.
[9] J. Svensson, N. Lindahl, H. Yun, M. Seo, D. Midtvedt, Y. Tarakanov, N. Lindvall, O. Nerushev, J. Kinaret, S. Lee, E. E. B. Campbell, *Nano Lett.* **2011**, *11*, 3569–3575.
[10] T. M. Barnes, J. D. Bergeson, R. C. Tennent, B. A. Larsen, G. Teeter, K. M. Jones, J. L. Blackburn, J. van der Lagemaat, *Appl. Phys. Lett.* **2010**, *96*, 243309.
[11] K. H. An, S. Y. Jeong, H. R. Hwang, Y. H. Lee, *Adv. Mater.* **2004**, *16*, 1005–1009.
[12] M. Terrones, *ACS Nano* **2010**, *4*, 1775–1781.
[13] D. V. Kosynkin, A. L. Higginbotham, A. Sinitskii, J. R. Lomeda, A. Dimiev, B. K. Price, J. M. Tour, *Nature* **2009**, *458*, 872–876.
[14] L. Jiao, X. Wang, G. Diankov, H. Wang, H. Dai, *Nat. Nanotechnol.* **2010**, *5*, 321–325.
[15] H. Santos, L. Chico, L. Brey, *Phys. Rev. Lett.* **2009**, *103*, 086801.
[16] A. L. Higginbotham, D. V. Kosynkin, A. Sinitskii, Z. Sun, J. M. Tour, *ACS Nano* **2010**, *4*, 2059–2069.
[17] I. K. Moon, J. Lee, R. S. Ruoff, H. Lee, *Nat. Commun.* **2010**, *1*, 73.
[18] Y. Xue, J. Liu, H. Chen, R. Wang, D. Li, J. Qu, L. Dai, *Angew. Chem.* **2012**, *124*, 12290–12293; *Angew. Chem. Int. Ed.* **2012**, *51*, 12124–12127.
[19] Z. Yang, L. Li, Y. Luo, R. He, L. Qiu, H. Lin, H. Peng, *J. Mater. Chem. A* **2013**, *1*, 954–958.

 © 2013 Wiley-VCH Verlag GmbH & Co. KGaA, Weinheim